AGU PUBLICATIONS

JGR

Journal of Geophysical Research: Oceans

RESEARCH ARTICLE

10.1002/2014JC009849

Key Points:
- Sea ice gas content was 27.5% O_2, 71.4% N_2, and 1.09% Ar, and gas is located in bubbles
- Gas transport in sea ice is controlled by diffusion during the winter
- The diffusion is the same order than the aqueous diffusion

Correspondence to:
O. Crabeck,
crabecko@myumanitoba.ca

Citation:
Crabeck, O., B. Delille, S. Rysgaard, D. N. Thomas, N.-X. Geilfus, B. Else, and J.-L. Tison (2014), First "in situ" determination of gas transport coefficients (D_{O_2}, D_{Ar}, and D_{N_2}) from bulk gas concentration measurements (O_2, N_2, Ar) in natural sea ice, *J. Geophys. Res. Oceans*, *119*, 6655–6668, doi:10.1002/2014JC009849.

Received 23 JAN 2014
Accepted 4 SEP 2014
Accepted article online 10 SEP 2014
Published online 7 OCT 2014

First "in situ" determination of gas transport coefficients (D_{O_2}, D_{Ar}, and D_{N_2}) from bulk gas concentration measurements (O_2, N_2, Ar) in natural sea ice

Odile Crabeck[1], B. Delille[2], S. Rysgaard[1,3,4], D. N. Thomas[5,6], N.-X. Geilfus[1,3], B. Else[1], and J.-L. Tison[7]

[1]Department of Geological Science, CEOS, University of Manitoba, Winnipeg, Manitoba, Canada, [2]Unité d'Océanographie Chimique, MARE, Université de Liège, Liège, Belgium, [3]Arctic Research Centre, Aarhus University, Aarhus, Denmark, [4]Greenland Climate Research Centre, Greenland Institute of Natural Resources, Nuuk, Greenland, [5]School of Ocean Sciences, Bangor University, Anglesey, UK, [6]Marine Research Centre, Finnish Environment Institute, Helsinki, Finland, [7]Laboratoire de Glaciologie, DSTE, Université Libre de Bruxelles, Bruxelles, Belgium

Abstract We report bulk gas concentrations of O_2, N_2, and Ar, as well as their transport coefficients, in natural landfast subarctic sea ice in southwest Greenland. The observed bulk ice gas composition was 27.5% O_2, 71.4% N_2, and 1.09% Ar. Most previous studies suggest that convective transport is the main driver of gas displacement in sea ice and have neglected diffusion processes. According to our data, brines were stratified within the ice, so that no convective transport could occur within the brine system. Therefore, diffusive transport was the main driver of gas migration. By analyzing the temporal evolution of an internal gas peak within the ice, we deduced the bulk gas transport coefficients for oxygen (D_{O2}), argon (D_{Ar}), and nitrogen (D_{N2}). The values fit to the few existing estimates from experimental work, and are close to the diffusivity values in water (10^{-5} cm^2 s^{-1}). We suggest that gas bubbles escaping from the brine to the atmosphere—as the ice gets more permeable during melt—could be responsible for the previously reported high transport coefficients. These results underline that when there is no convective transport within the sea ice, the transport of gas by diffusion through the brines, either in the liquid or gaseous phases, is a major factor in controlling the ocean-atmosphere exchange.

1. Introduction

To date, only a limited number of studies describing the natural gas composition of sea ice are available [e.g., *Matsuo and Miyake*, 1966; *Rysgaard and Glud*, 2004; *Tison et al.*, 2002; *Zhou et al.*, 2013]. These studies typically found a total gas content lower than 23.75 mL STP kg^{-1} ice—a value expected if seawater is instantly frozen—and reported bulk ice gas compositions on the order of $\approx 1/3$ O_2 and $\approx 2/3$ N_2, similar to atmospheric and seawater compositions. The formation of these gas inclusions has been described in detail by *Tsurikov* [1979] who identified nine key processes that trap gases in sea ice. Most importantly, during the freezing process, the expelled dissolved gases are trapped in the brines or in bubbles that are released at the ice-water interface (Figure 1: initial gas entrapment). Increased concentrations of solutes in brines by freezing results in further formation of gas bubbles by nucleation processes (Figure 1: postgenetic process). More gas inclusions can be created during sea ice melt, as water vapor forms inside the brine pockets above the freeboard line. Finally, drained bine pockets and channels may be replaced by atmospheric gases.

The presence of a gas phase in sea ice creates the potential for gas exchange with the atmosphere, although unfortunately gas transfer at the sea ice-atmosphere interface is not well constrained [*Else et al.*, 2011; *Heinesch et al.*, 2009; *Loose et al.*, 2011; *Miller et al.*, 2011; *Papakyriakou and Miller*, 2011; *Sørensen et al.*, 2013; *Zemmelink et al.*, 2006]. For example, studies have shown that sea ice can act as a source [e.g., *Geilfus et al.*, 2012, 2013; *Miller et al.*, 2011; *Nomura et al.*, 2006] or a sink for atmospheric CO_2 [e.g., *Nomura et al.*, 2010; *Papadimitriou et al.*, 2012; *Rysgaard et al.*, 2007; *Zemmelink et al.*, 2006], with the reported fluxes spanning several orders of magnitude.

Three main processes should be considered for gas transport within sea ice (Figure 1: transport): (a) convection with the brine medium, (b) diffusion along the concentration gradient (in the dissolved state within the brine medium), and (c) upward gas movement under buoyancy (in the gaseous state

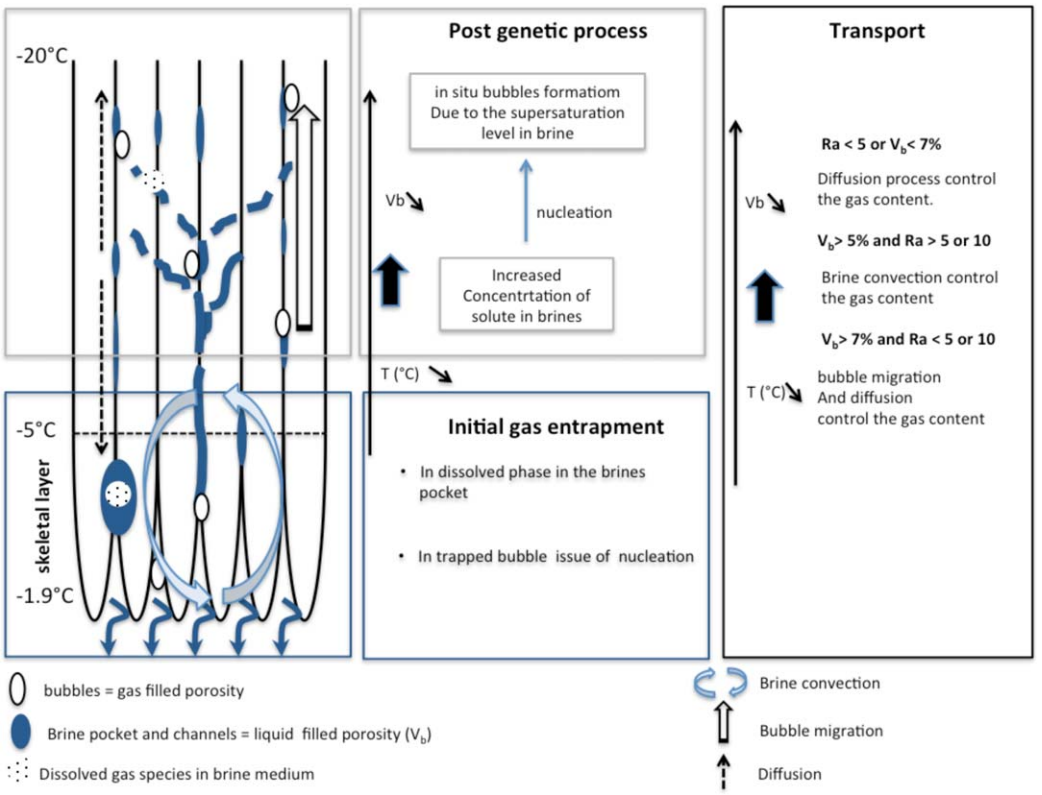

Figure 1. Schematic view of gas entrapment and evolution in sea ice. During the freezing process, the expelled dissolved gases are trapped in the brine solution, or in bubbles that are released at the ice-water interface. Increased concentration of the brines by freezing results in further formation of gas bubbles by nucleation processes. The main transport processes of gas within the sea ice depend on the permeability and convection threshold given by the brine volume and the Rayleigh number. If V_b is under 5%, no convection occurs in sea ice and gas transport is controlled by diffusion process. During diffusion, the gas can be released both into the underlying water and to the atmosphere as a function of the gradient concentration. While V_b is above 5% and Ra $>$ 5 or 10, brine convection occurs and brine can exchange with the seawater underneath. If the V_b exceeds 7.5%, bubbles are able migrate upward and gas maybe released to the atmosphere.

within the brine medium). All three require that there is a certain level of permeability in the sea ice, which may differ depending on the process considered. According to *Golden et al.* [1998, 2007], the permeability of sea ice rapidly increases when the brine volume fraction exceeds 5%. At brine volume fractions below 5%, no brine convection is expected to occur, and the ice cover is often considered impermeable to gas exchange. A recent study by *Zhou et al.* [2013] suggests that a brine volume of ~7% is required for upward bubble migration (through bubble buoyancy). These observations are consistent with *Loose et al.* [2011] who suggest that the permeability threshold for gas transport could be different from the permeability threshold for brine convection (i.e., gravity drainage) or bubble migration. Past studies [*Gosink et al.*, 1976; *Loose et al.*, 2009, 2011; *Shaw et al.*, 2011] have actually suggested that diffusion is the major control on gas fluxes across sea ice, and it appears to be active even at low brine volumes. Diffusive transport through the porous structure of sea ice is therefore an alternative pathway for ocean-atmosphere exchange of gases in the absence of convection processes (i.e., brine drainage under brine density instability).

The aim of the present study was to examine the physical processes that affect mass transport of biogenic gases across and within sea ice. Unlike previous studies, which have used artificial gas tracers [e.g., *Gosink et al.*, 1976], or artificial sea ice [e.g., *Loose et al.*, 2011], we used measurements of natural gas concentrations in natural sea ice samples. By studying the temporal evolution of the vertical profile of O_2, N_2, and Ar, we were able to compute diffusivities of these gases in a natural environment. Since only one study [*Gosink et al.*, 1976] reports such measurements in natural environment, our findings significantly enhance scientific understanding of gas transport in sea ice. Furthermore, our observations can be used to validate previous studies made in the laboratory and other experimental settings.

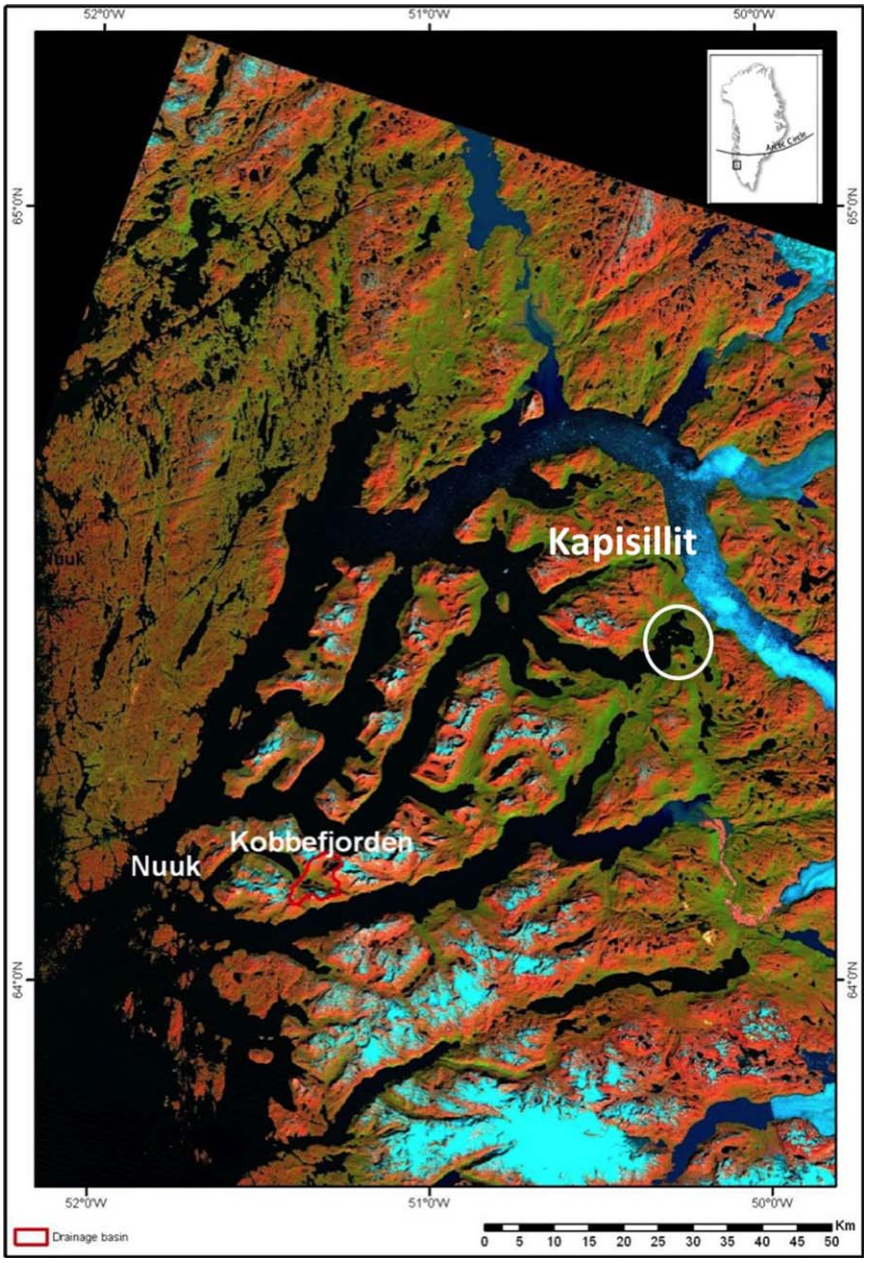

Figure 2. Study site—Landfast sea ice in Godthåbsfjord, SW Greenland. Circle includes the Bay with the study site and the settlement Kapisillit.

2. Study Site

The sampling was conducted from 10 to16 March 2010 on first-year landfast sea ice in Kapisillit in the vicinity of Nuuk, SW Greenland (64°26′N 50°13′W, Figure 2). To follow the temporal evolution of the sea ice, we sampled sea ice and the underlying water column four times at the same site on three occasions: 11 March, 13 March, and 15 March. Sampling was performed within an area of about 25 m^2 in order to minimize bias from spatial heterogeneity. The water depth at the location ranged from 40 to 45 m, and the mean salinity of seawater in the Kapisillit fjord was 32. The air temperatures during the study period ranged from −8.8°C to +2.9°C (average −3.2°C). The survey took place before the onset of the spring algal bloom: concentrations of chlorophyll-a were 2.8 ± 0.4 $\mu g\ L^{-1}$ (SE, n = 3) in the bottom 12 cm of ice, while the average concentration across the entire ice thickness was 1.0 ± 1.2 $\mu g\ L^{-1}$ (SE, n = 3) [*Long et al.*, 2012; *Sogaard et al.*, 2013].

3. Methods

3.1. Sea Ice Temperature, Salinity, and Texture

Ice cores were extracted using a stainless-steel corer with an internal diameter of 9 cm (Kovacs Ent., Lebanon, USA). Cores were immediately wrapped in polyethylene bags and stored at the sampling site in an insulated box filled with individual cooling bags precooled at −20°C. In the laboratory, ice cores were kept at −20°C in the dark to ensure brine/gas immobilization and to inhibit biological processes [*Eicken et al*., 1991]. On a replicate core extracted from the same location, in situ ice temperature was measured with a depth resolution of 5 cm, using a calibrated probe (Testo 720) inserted into predrilled holes (with the same diameter as the probe) perpendicular to the ice core axis. The precision of the probe was ±0.1°C. This "temperature" ice core was immediately cut into 5 cm slices, stored in polyethylene buckets, and left to melt. Back in the laboratory, bulk ice salinity was measured with a portable conductivity meter (Orion Star Series Meter WP-84TP) with a precision of ±0.1. To describe the texture of the ice, horizontal thin sections were produced in 10 cm sections from a third ice core, using the standard microtone (Leica SM2400) following the procedure described by *Langway* [1958] and *Tison et al*. [2008]. The images from horizontal thin sections were collected with a digital camera (Nikon Coolpix S200, 7.1 megapixels) between crossed polarizers.

3.2. Total Gas Content

The total volume of gas within sea ice (content in mL STP of gas per kg of ice) was measured with a resolution of 5 cm using the wet extraction method [*Raynaud et al*., 1982]. In short, ice samples from the retained core were placed in an evacuated glass container. The ice was then melted and refrozen from the bottom using a −70°C cold ethanol bath. This technique of melting-refreezing releases both the dissolved gas in the brine and the gas content from the bubbles [*Tison et al*., 2002]. After the refreezing, the container was connected to a Toepler pump extraction system, and the entire gas volume was directed through a prevacuumed line to a mercury-graduated burette. Knowing the exact weight of the sample analyzed, the ice temperature, and atmospheric pressure, we calculated the STP gas content of the sample with a precision of ±5%.

3.3. Gas Composition

Argon (Ar), oxygen (O_2), and nitrogen (N_2) were analyzed by gas chromatography. Extraction of the gas phase from the ice used the dry-crushing technique as developed for gas measurements in continental ice [*Raynaud et al*., 1982]. Each ice core was cut in successive 5 cm sections, and 60 g of each section was put into a vessel together with stainless-steel beads. The vessel was evacuated to 10^{-3} torr, and then fixed to an ice crusher as described in *Raynaud et al*. [1982] and *Stefels et al*. [2012]. The stainless-steel beads impact the ice block during the shaking process, so that the ice is crushed into a fine powder. The cutting and shaking processing took place in a cold room at −25°C. After crushing, the vessel was kept at −50°C in a cold ethanol bath, and connected to a gas chromatograph equipped with a thermal conductivity detector for concentration analyses [*Skoog et al*., 1997]. We used AlphagazTM2 He (Air Liquid–P0252) as the carrier gas and a 22 mL packed column (Mole Sieve 5A 80/100; 5 m × 1/8″). The gas collected included both the gas bubbles in the ice and the dissolved phase within liquid brines.

We compared the evolution of Ar, O_2, and N_2 concentration in bulk ice to the inventory constrained by the solubility in brine at atmospheric saturation. The latter represents the maximum concentration of Ar, O_2, and N_2 in the dissolved phase, if no supersaturation existed in the brine [*Carte*, 1961; *Lubetkin*, 2003, *Zhou et al*., 2013]. It is obtained by calculating the temperature and salinity-dependent solubility of Ar, O_2, and N_2 in the brines [*Garcia and Gordon*, 1992; *Hamme and Emerson*, 2004] and dividing it by the relative brine volume (brine volume fraction *b/V*, see below) to express it as micromoles per liter of bulk ice. *Zhou et al*. [2013] showed than these relationships remain valid for the range of temperature and salinity found in sea ice. The difference between observed concentration in bulk ice ($C_{bulk\ ice}$) and the theoretical saturation concentration in brine ($C_{saturation}$) provides a maximum estimate of the gas concentration in the ice that resides in the gas phase, C_B (i.e., the gas content of bubbles, assuming no super saturation in the brines):

$$C_B = C_{bulk\ ice} - C_{saturation} \quad (1)$$

We also calculated the supersaturation factor, (Sat_f):

$$Sat_f = {}^{C_{bulk\ ice}}/_{C_{saturation}} \quad (2)$$

and the percent gas content in the bubbles, (f_B):

$$f_B = \left({}^{C_B}/_{C_{bulk\ ice}}\right) \times 100 \quad (3)$$

3.4. Liquid/Gas-Filled Porosity and Rayleigh Number

The brine volume, (b), was calculated according to *Cox and Weeks* [1983] for ice temperature $< -2°C$ and according to *Leppäranta and Manninen* [1988] for ice temperature $\geq -2°C$, neglecting the gas-filled porosity. Brine salinity, (S_b), was calculated from the measured sea ice temperatures and freezing point of seawater [*UNESCO*, 1978]. The brine volume fraction or gas-filled porosity, (V_b), was calculated as brine volume/bulk sea ice volume (*b/V*, expressed in %).

The bubble volume (L gas phase per L of ice), (*B*), was determined by multiplying C_B by the gas molar volume using gas law normalized at the average ice temperature ($-3.2°C$) ($Vm = 22.14 \times 10^{-6}$ L mol^{-1}), and summing the contribution of all gas species:

$$B = C_B \times Vm \quad (4)$$

The gas-filled porosity or bubble volume fraction was calculated as a percentage of the volume total of ice, V_B:

$$V_B = \left({}^{B}/_{Bulk\ ice\ volume}\right) \times 100 \quad (5)$$

This calculated value is a maximum percentage, supposing that no supersaturation existed in the brines, and only considering O_2, N_2, and Ar concentrations in the ice. Note also that this value is slightly underestimated since C_B is calculated from $C_{saturation}$ (equation (1)), itself overestimated since we neglected the gas-filled porosity in the use of *Cox and Weeks* [1983] formulation to estimate the brine volume fraction. *Cox and Weeks* [1983] estimated the gas-filled porosity to be between 1% and 5%.

The Rayleigh number is a parameter that primarily determines the onset of convection (e.g., gravity drainage) and provides information about the vertical stability in the brine system. The Rayleigh number (Ra) was estimated using the definition of *Notz and Worster* [2008].

4. Results

4.1. Physical Ice Properties

Detailed physical properties of the sea ice cores are presented elsewhere [*Crabeck et al.*, 2014; *Kaartokallio et al.*, 2013; *Sogaard et al.*, 2013]. In short, the ice consisted of columnar crystals, and was relatively warm throughout, with a slight temperature gradient (Figure 3a) from top (-2.8 to $-3.8°C$) to bottom (-0.8 to $-1.2°C$). The ice was covered by a thin layer of frozen snow, less than 3 cm thick during all the sampling period. The average bulk ice salinity was 3.2, and the ice salinity profiles deviated from the classical C-shape due to a variable localized riverine input (Figure 3b). During the survey, the brine volume fraction fell below the permeability threshold of 5% at various depths (Figure 3c), indicating that the atmosphere was not effectively connected to the seawater through the ice. Furthermore, the Rayleigh number ranged from 0 to 0.3 (Figure 3d), and remained well below the theoretical convection threshold of 5 [*Vancoppenolle et al.*, 2010] or 10 [*Notz and Worster*, 2008] throughout the ice. Thus, we do not expect that convective transport of brine occurred at anytime, or at any level of the sea ice. However, the V_b exceeds 30% in the bottom of the ice (Figure 3c), and there was no brine convection because the driving buoyancy given by the brine density gradient was not large enough to overcome dissipation.

4.2. Gas Composition

At all dates, the total gas content in sea ice ranged from 4 to 23.2 mL STP kg^{-1} ice, consistently lower than the 23.75 mL STP kg^{-1} ice expected for instantly frozen seawater [*Cox and Weeks*, 1983]. This is consistent with past

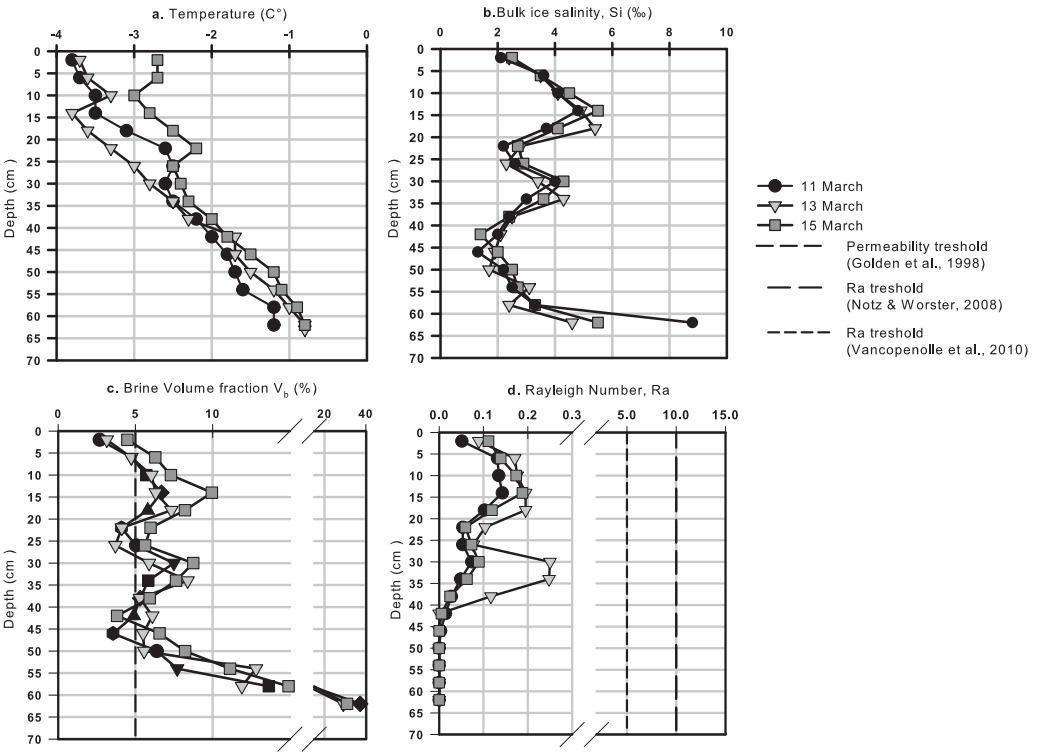

Figure 3. (a) Bulk ice salinity, S_i, (b) temperature, (c) brine volume fraction or liquid-filled porosity, V_b. The vertical dashed line is a reference value for the permeability threshold according to *Golden et al.* [1998, 2007], (d) Rayleigh number, Ra, and the dotted lines are a reference value for the convection threshold according to *Notz and Worster* [2008] and *Vancoppenolle et al.* [2010], respectively.

findings [e.g., *Tison et al.*, 2002], and is a result of the rejection of gases during ice formation. Furthermore, a peak in gas content in the ice was observed between 25 and 35 cm below the surface at all sampling dates (Figure 4a).

Mixing ratios in sea ice ranged from 0.94% to 1.29% for Ar, 22.4% to 32.9% for O_2, and 68.9 to 76.6% for N_2 (Table 1). These correspond to a bulk ice Ar concentration of 1.3–11.7 μmol L^{-1} ice (average 5.4 μmol L^{-1} ice), a bulk ice O_2 concentration of 40–275 μmol L^{-1} ice (average 132 μmol L^{-1} ice), and a bulk ice N_2 concentration of 57–830 μmol L^{-1} ice (average 354 μmol L^{-1} ice). Each gas profile (for each sampling date) had minimum concentrations in the bottom of the sea ice and a peak around 27 cm below the ice surface (Figure 5).

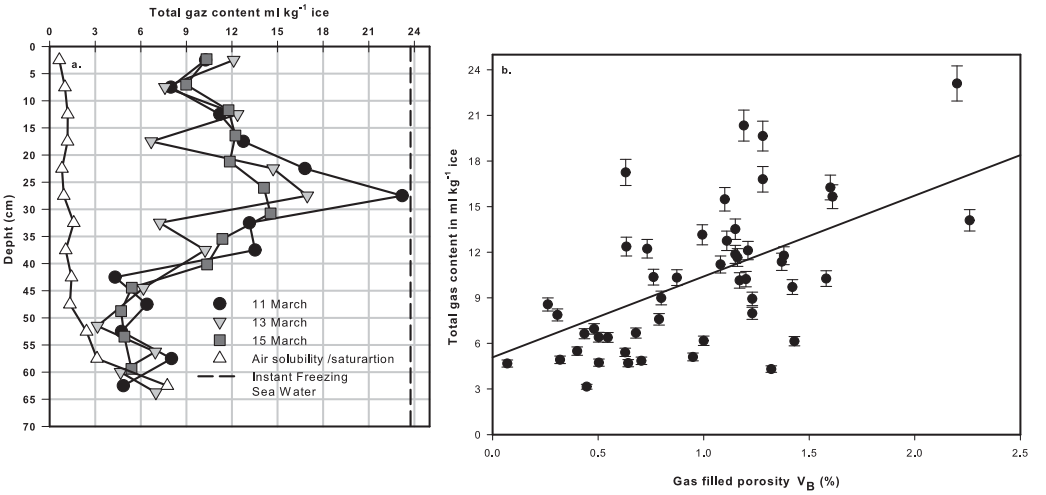

Figure 4. (a) Evolution of the total gas content in bulk sea ice as compared to solubility in brine at atmospheric saturation (white circle; air solubility). (b) Relationship between the total gas content measured with the Toepler pump and the computed gas-filled porosity (V_B). A regression line is shown ($r^2 = 0.37$, $P < 0.001$) and its intersection with the y axis represent the maximum volume of dissolved gas in the brines.

Table 1. Relative Proportion of O_2, Ar, and N_2 in Landfast Sea Ice at Kapisilit

	O_2		Ar		N_2	
Gas Composition (%)	Min	Max	Min	Max	Min	Max
11 Mar	22.7	32.7	0.94	1.28	68.2	76.3
13 Mar	23.9	31.4	0.970	1.25	67.2	75.1
15 Mar	24.1	30.5	0.973	1.29	68.2	74.9
Sea ice [*Tsurikov*, 1979]	20.6	29.0	0.9	1.1	54.2	76.8
Sea ice [*Tison et al.*, 2002]	24.36	30.46	nd	nd	69.54	78.08
Sea water (t = 0°C, S = 33)	34.84		1.69		61.14	
Atmospheric composition	20.95		0.93		78.08	

Over time, the O_2, N_2 and Ar gas peaks decreased. Between 11 and 13 March, O_2 and Ar concentrations decreased by 13.9 and 13.6%, respectively, while N_2 concentrations decreased 3 times faster (32.1%).

Each gas species exceeded the concentrations calculated at atmospheric saturation (Table 2). The saturation factor (Sat_f) (equation (2)) varied from 0.82 to 39 for N_2, from 0.64 to 20.2 for O_2, and from 0.52 to 18.5 for Ar. Maximum supersaturation factors were systematically observed in the middle of the ice, 27.5 cm below the ice surface, while the minimum was observed in the permeable bottom 5 cm of the ice (Table 3). N_2 was the most supersaturated gas species, with an average saturation factor of 9.16, compared to 6.88 for O_2, and 5.05 for Ar. According to equation (3), more than 70% of the gas species were in the gas phase while less than 30% was dissolved in the brine (Table 3).

Overall, the liquid-filled porosity represented 3–8% of the ice volume (Table 3), except in the bottom 5 cm where V_b exceeded 30%. The calculated gas-filled porosity was at most 2.2% of the ice volume, and it was equal, or close, to 0 in the bottom 5 cm. This means that all gas species were dissolved in the brine in the bottom horizons of the sea ice. The total porosity varied from 4 to 12%, except in the bottom 5 cm where it exceeded 30%.

5. Discussion

5.1. Gas Profiles

All sampling dates showed a peak of gas content between 25 and 35 cm depth, which decreased over time. As the fjord is periodically influenced by riverine input [*Mortensen et al.*, 2011], this layer could be formed during periods with freshwater flowing under the growing ice. This would create fresher, less permeable ice layers and at the same time increase the total gas content due to the higher gas content in freshwater relative to seawater (Figures 3a and 5).

Gas profiles in sea ice result from both physical and/or biological processes. Ar is an inert gas and therefore is not involved in biogeochemical processes, and so it can be used as a tracer of physical processes involved in gas concentration and transport within sea ice [*Zhou et al.*, 2013]. In contrast, O_2 and N_2 are biogenic gases and

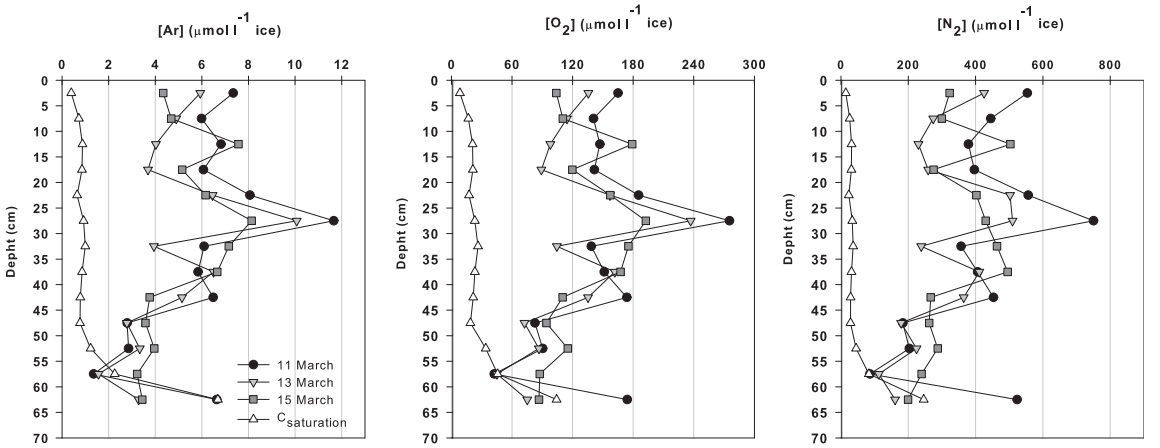

Figure 5. Evolution of Ar, O_2, and N_2 concentrations in bulk sea ice as compared to the concentration at atmospheric saturation (white triangle).

Table 2. Saturation Factor, (Sat_f), Computed Following the Equation (2)

Gas Species	Saturation Factor ($C_{bulkice}/C_{saturation}$)	
	Min	Max
O_2	0.64	20.2
Ar	0.52	18.5
N_2	0.82	39

their dynamics involve both physical and biogeochemical processes. In seawater, the Ar:O_2 ratio is commonly used to remove the physical contribution to oxygen supersaturation and to determine the biological oxygen production [e.g., *Cassar et al*., 2009; *Castro-Morales et al*., 2013]. However, the strong correlation ($r^2 > 0.89$, $P \leq 0.01$) between Ar and both O_2 and N_2 in this study (Figure 6) suggests that physical transport processes mainly controlled the gas compositions within the sea ice, biological processes only having a minor effect. These observations are in agreement with the abiotic laboratory sea ice experiment described by *Tison et al*. [2002]. In addition, *Sogaard et al*. [2013] have shown that the total dissolved inorganic carbon within the ice cover in the same area was mainly controlled by physical export via brine drainage and the precipitation/dissolution of calcium carbonate rather than biological processes.

The relative proportion of O_2, Ar, and N_2 in bulk sea ice in this study are intermediate between the relative gas composition in dissolved seawater and the atmospheric gas composition (Table 1 and Figure 6). These results are in agreement with the past studies of *Matsuo and Miyake* [1966] and *Tison et al*. [2002] and reflect the mixed contribution of the dissolved and gaseous fractions of each gas, with the dominance of the gaseous (bubble) fraction (as also shown by the regression line in Figure 6 being closer to the atmospheric ratio and the f_B values in Table 3). Each gas species in the bottom ice layers was close to, or below, atmospheric saturation (Figure 5), confirming the results of *Zhou et al*. [2013] that the gas incorporation at the ice-water interface occurs close to the atmospheric solubility value.

The ice was enriched in N_2 (i.e., highest saturation factor) compared to O_2 and Ar (Table 2). The gas composition is a function of a chemical separation of gases diffusing across the boundary layer at the ice-water interface during the ice growth [*Carte*, 1961; *Killawee et al*., 1998; *Loose et al*., 2009, 2011; *Tison et al*., 2002]. Because the N_2 diffusion coefficient is lower than the O_2 and Ar diffusion coefficients, the flux of N_2 from sea ice to the water is slower and, hence, the incorporation rate of N_2 is larger than O_2 and Ar, leading to N_2 enrichment within sea ice.

Moreover, solubility of N_2 is only half the solubility of O_2 if nucleation process occurs at the ice-water interface. This results in relatively more N_2 in the gas phase as compared with the other gases. The growing ice will therefore be enriched in nitrogen bubbles that would otherwise have diffused as a solute toward the water reservoir.

Table 3. Temporal Evolution of Sea Ice Properties at the Gas Maximum[a]

	a. 11 March			b. 13 March			c. 15 March		
	Mean Depth (cm)			Mean Depth (cm)			Mean Depth (cm)		
	22.5	27.5	32.5	22.5	27.5	32.5	22.5	27.5	32.5
T(°C)	−2.59	−2.54	−2.54	−3.26	−2.92	−2.61	−2.24	−2.46	−2.34
Bulk salinity	2.25	3.12	3.37	2.74	2.67	3.96	2.72	3.42	3.95
V_b (%)	4.2	5.97	6.45	4.00	4.48	7.36	5.93	6.75	8.05
$C_{bulk\ ice}$, O_2 (μmol L^{-1} ice)	185.34	275.30	138.46	156.98	236.99	104.47	157.39	192.53	175.34
$C_{bulk\ ice}$, N_2 (μmol L^{-1} ice)	556.15	750.16	356.72	502.57	509.60	238.42	402.63	429.87	463.61
$C_{bulk\ ice}$, Ar (μmol L^{-1} ice)	8.06	11.66	6.10	6.461	10.07	3.95	6.16	8.14	7.16
$C_{saturation}$, O_2 (μmol L^{-1} ice)	13.29	18.97	20.50	11.94	13.66	23.21	19.45	21.64	26.13
$C_{saturation}$, N_2 (μmol L^{-1} ice)	23.43	33.48	36.18	20.89	24.00	40.92	34.44	38.21	46.22
$C_{saturation}$, Ar (μmol L^{-1} ice)	0.65	0.92	1.00	0.58	0.66	1.13	0.95	1.05	1.27
C_B, O_2 (μmol L^{-1} ice)	172.05	256.32	117.96	145.04	223.26	81.27	137.95	170.89	149.21
C_B, N_2 (μmol L^{-1} ice)	532.72	716.68	320.54	481.69	485.60	197.51	368.19	391.66	417.39
C_B, Ar (μmol L^{-1} ice)	7.42	10.74	5.10	5.88	9.40	2.82	5.22	7.08	5.88
f_B, O_2 (%)	92.83	93.11	85.19	92.39	94.23	77.78	87.64	88.76	85.10
f_B, N_2 (%)	95.79	95.54	89.86	95.84	95.28	82.83	91.45	91.11	90.03
f_B, Ar (%)	91.97	92.07	83.61	90.99	93.38	71.33	84.61	87.04	82.20
B, O_2 (L gas L^{-1} ice)	0.0038	0.0057	0.0026	0.0032	0.0049	0.0018	0.0031	0.0038	0.0033
B, N_2 (L gas L^{-1} ice)	0.0118	0.0159	0.0071	0.0107	0.0108	0.0044	0.0082	0.0087	0.0092
B, Ar (L gas L^{-1} ice)	0.0002	0.0002	0.0001	0.0001	0.0002	0.0001	0.0001	0.0002	0.0001
V_B (%)	1.6	2.22	0.98	1.40	1.59	0.62	1.13	1.26	1.27
Total porosity (air + brine) (%)	5.78	8.15	7.43	5.45	6.07	7.98	7.06	8.01	9.32

[a]The reported values are sea ice temperature (T), relative brine volume (V_b), bulk ice gas concentration ($C_{bulk\ ice}$), saturation concentration in brine ($C_{saturation}$), gas concentration in bubbles (C_B), the fraction of gas content in bubble (f_B), the bubble volume (B), and relative bubble volume or gas-filled porosity (V_B).

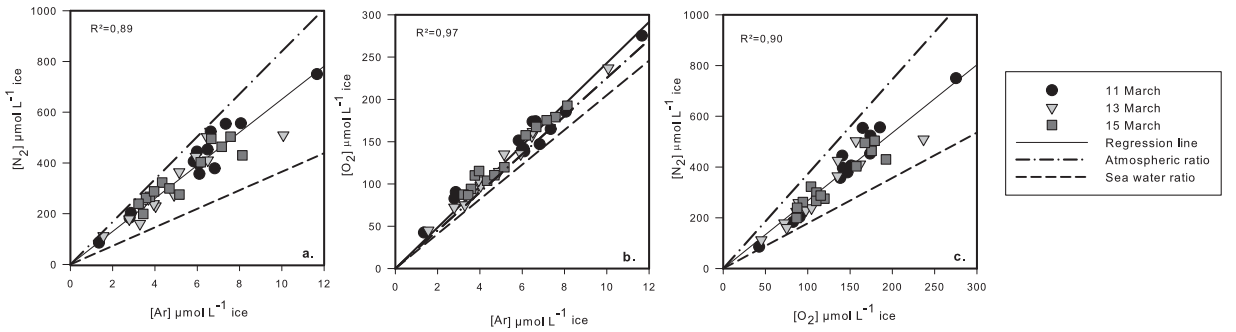

Figure 6. Relationship between N_2, O_2, and Ar in the sea ice samples. The solid line is the regression line. The solid line represents the sea water ratios (N_2:Ar, O_2:Ar, N_2:O_2) while the dashed line represents the atmospheric ratios (N_2:Ar, O_2:Ar, N_2:O_2).

5.2. Gas Porosity and Bubble Formation From Brine Supersaturation

The estimated gas-filled porosity (V_B) was 1–2.2% of the ice volume (Table 3). These estimates are in the lower end of the estimates (1–5%) based on *Cox and Weeks* [1983], but are close to the range (1.3–1.9%) reported by *Loose et al.* [2011]. Figure 4b shows that the total gas content in sea ice is linearly related to bubble volume ($R^2 = 0.37$; $P \leq 0.01$, Figure 4b). We used this relationship to infer that at $B = 0$ (i.e., no bubbles are present), the total gas content (which must be contained exclusively in the brines) would be approximately 5.6 mL kg^{-1}. This implies that gas comes out of solution to form bubbles when the gas concentration in the brines exceeded this value. The average air solubility of the brine medium was 2.06 mL $kg^{-1} \pm 0.91$, so nucleation within the sea ice system appeared at saturation factor between 1.9 and 4.9. These results are comparable to the findings of *Killawee et al.* [1998] in freshwater, who observed bubble nucleation when saturation was between 2.2 and 2.5 times atmospheric saturation at the ice-water interface. Note that the relatively low R^2 of the relationship between gas porosity and total gas content (Figure 4b) is not surprising given the potential bias affecting both methods: first, total gas content and C_B (which is used to reconstruct the gas-filled porosity (V_B)) were measured on two different cores; second, the C_B estimate is calculated from equation (1), in which $C_{saturation}$ is derived from a brine volume fraction estimate that does not take into account the air content (i.e., it is a simplification of the *Cox and Weeks* [1983] formulation).

5.3. A First Assessment of Gas Transport Coefficients in Sea Ice at Constant Brine Volume

For each gas, we observed a decreasing peak with time at 27.5 cm below the ice surface (Figure 5). This gradual decrease of the gas concentration suggests that there was a gas movement within the sea ice. The gas species displaced symmetrically from the highest concentration situated at 27.5 cm below the ice surface to lower concentration. Given the fact that the ice was not affected by brine convection mechanisms (see section 4.1, Figure 3d), the mode of transportation was either through molecular diffusion in the brine (aqueous diffusion) or bubble buoyancy. A distinguishing feature of diffusion is that it results in mixing or mass transport, without requiring bulk motion. In the phenomenological approach, according to Fick's laws, the diffusion flux is proportional to the negative gradient of concentrations. It goes from regions of higher concentration to regions of lower concentration. The Fick's second law of diffusion describes the change of concentration with time as:

$$\frac{\partial C_{bulk\ ice}}{\partial t} = D\left(\frac{\partial^2 C_{bulk\ ice}}{\partial z^2} + \frac{1}{A}\frac{\partial A}{\partial z}\frac{\partial C_{bulk\ ice}}{\partial z}\right) \quad (6)$$

Where $C_{bulk\ ice}$ is the bulk ice concentration in μmol L^{-1} (= nmol cm^{-3}), t is the time in s, D is the diffusion coefficient expressed in $cm^2\ s^{-1}$, z is the length in cm, and A is the cross-sectional area over which diffusion is occurring in cm^2.

The diffusion of gas within sea ice is thought to occur through the network of brines. Assuming the brine network can be described as a tube perpendicular to the ice cover (i.e., z direction) of section area, A, the geometry of the problem is similar to decay of a pulse [*Cussler*, 2009, p. 34]. In the decay of pulse model, the diffusion occurs away from a sharp pulse of solute (i.e., the gas peak at 27.5 cm below the ice surface). The initially steep concentration gradient weakens gradually by diffusion in the z direction (i.e., the brine channel perpendicular to the ice cover) into the smooth curves.

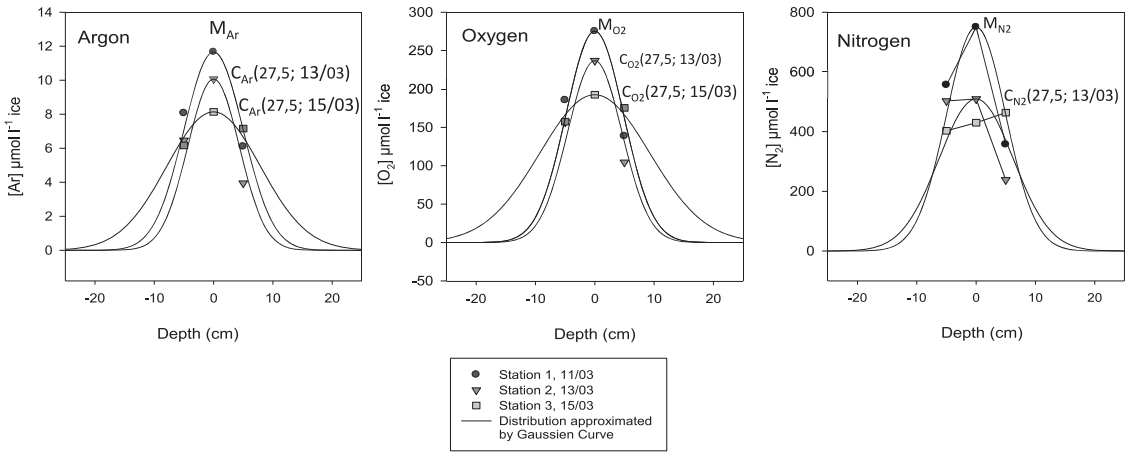

Figure 7. Best fit curves of the gas peak situated at 27.5 cm below the ice surface. For each species, the concentration distribution is approximated by a Gaussian curve fit with three parameters.

For this first estimate of *D* values, we assumed that diffusion occurs in a one-dimensional medium of infinite length where the cross-sectional area is considered as constant. This cross-sectional area is the brine network, and since the V_b only varied between 2 and 3% during the sampling period, we can assume it was constant. Hence, the third term of the second Fick's law, $\left(\frac{1}{A}\frac{\partial A}{\partial z}\frac{\partial C_{bulk\ ice}}{\partial z}\right)$ (equation (6)) is zero.

We approximated the vertical gas concentrations around the peak as a normal distribution (Figure 7) by applying a curve fit procedure that assumes that the concentrated solute was originally located at z = 0 (i.e., 27.5 cm below the ice surface), and diffused as per the Gaussian profile where the mathematical solution for the decay of pulse is given by:

$$\bar{C} = \frac{M\ /A}{\sqrt{4\pi Dt}} e^{-z^2/4Dt} \tag{7}$$

where *M* is the total solute introduced in the system, A is the cross-sectional area in cm, *Z* is the length of the system over which the solute diffuses in cm, *D* is the diffusion coefficient expressed in cm^2 s^{-1}, and *t* is the time expressed in s. The boundary conditions for this equation are as follows: (1) far from the pulse, the solute concentration is zero: $t > 0$; $z = \infty$; $C = 0$; (2) because diffusion occurs at the same speed in both directions (constant section), the pulse is symmetric; (3) all of the solute is initially located at z = 0. At position z = 0, the evolution of the peak concentration over time is given by:

$$C(0,t) = \frac{M}{\sqrt{4\pi Dt}} \times dz \tag{8}$$

Where dz is the length of the section on which the gas concentration is measured, 5 cm. *C*(0,t) is the gas concentration successively measured on 13 March and on 15 March, 27.5 cm below the ice surface (Z = 0), (27.5, 13 March), C (27.5, 15 March), respectively. *M* is the total quantity introduced in the system, calculated from the maximum concentration observed on 11 March, 27.5 cm below the ice surface (Table 3).

From equation (8), we can then compute values of D for each gas species as:

$$D = \frac{\left(\frac{M}{C(0,t)} \times dz\right)^2}{4\pi t} \tag{9}$$

In this first approach, computed D_{Ar} ranged from 1.54 to 1.76 $\times$ 10^{-5} cm^2 s^{-1} ($\pm$17%), D_{O_2} from 1.54 to 1.77 $\times$ 10^{-5} cm^2 s^{-1} ($\pm$11%), and D_{N_2} equal to 2.49 $\times$ 10^{-5} cm^2 s^{-1} ($\pm$8%) (Table 4). We computed D_{N_2} only for the first period because, the peak decreased faster and asymmetrically, suggesting that other processes are involved.

5.4. Gas Diffusion Pathways and Bubble Buoyancy

As described above, there are two mechanisms for gas transport in sea ice in the absence of brine convection: (1) the dissolved gas can diffuse in the brine solution following the concentration gradient, or (2)

Table 4. Diffusivity Coefficients Deduced From Equations (8) and (9), and Comparison Reference Values in the Literature

Data			
Gas peak 27.5 (cm)	11 March	13 March	15 March
Z = 0	M	C (0, 13 Mar)	C (0,15 Mar)
[Ar] μmol L^{-1} ice	11.66	10.7	8.13
[O_2] μmol L^{-1} ice	275.3	236.9	192.5
[N_2] μmol L^{-1} ice	750.1	509.6	429.8
Results			
Diffusion in sea ice	D_{Ar} 10^{-5} cm^2 s^{-1}	D_{O_2} 10^{-5} cm^2 s^{-1}	D_{N_2} 10^{-5} cm^2 s^{-1}
Kapisilit ($-3.5 > T$ (°C) < -2; 5,4% $< V_b <$ 8.05%)	1.54–1.76 (±17%)	1.55–1.74 (± 9%)	2.49 (±11%)
References			
Diffusion in water	D_{Ar} 10^{-5} cm^2 s^{-1}	D_{O_2} $10^{-5}$$cm^2$ s^{-1}	D_{N_2} 10^{-5} cm^2 s^{-1}
Broecker and Peng [1974] (T = 0°C)	0.88	1.17	0.95
Stauffer et al. [1985] (T =0°C)	Na	2.08	1.61
Wise and Houghton [1966] (T=10°C)	1.7	1.7	1.8
Diffusion in sea ice	D_{SF_6} 10^{-5} cm^2 s^{-1}	D_{O_2} 10^{-5} cm^2 s^{-1}	D_{CO2} 10^{-5} cm^2 s^{-1}
Gosink et al. [1976] ($-15 > T$ (°C) < -7)	0.9	Na	40
Loose et al. [2011] ($-12 > T$ (°C) < -4; 6% $< V_b <$ 8%)	13 (±40%)	3.9 (±41%)	Na
Diffusion in gas phase [*Cussler*, 2009, 3rd ed.]		10^{-1} $cm^2 s^{-1}$	

the bubbles can move upward along the grain boundaries and in the brine network under buoyancy [*Loose et al*., 2011; *Zhou et al*., 2013]. If bubbles are mobile, we expect (1) a faster net gas transport (i.e., higher calculated diffusivities) and (2) a preferential apparent diffusion in the positive (upward) direction. Our computed transport coefficients are of the same magnitude as the aqueous molecular diffusion values (1 to 2 $\times$ 10^{-5} cm^2 s^{-1}) at similar temperatures (Table 4). This suggests that the gas species primarily diffused through the brine channels in the dissolved phase. However, according to equations (1) and (3), more than 70% of the gas species were residing in bubbles (as a maximum estimate). The observed symmetrical distribution of the gas around zone of the peak through time also suggests that the bubbles remained immobile. An explanation for this observation is that the permeability of the bulk ice was too low to allow for differential bubble movement under buoyancy. *Zhou et al*. [2013] have recently demonstrated that brine volumes higher than 7% are necessary for bubble differential movement in the brine network, as a result of tortuosity. Figure 3c shows that this condition was not fulfilled above 50 cm depth (the area of interest), at least for the 11 and 13 March measurements. The observed increase in brine volume fraction between 13 and 15 March is consistent with higher calculated diffusivities (some bubbles might actually have escaped and accumulated within the less permeable top 5 cm) (Figures 3c and 5).

Overall, our estimates of the gas retained in bubbles as a proportion of bulk ice gas concentrations, and the estimated gas-filled porosities are probably overestimates. According to *Light et al*. [2003], bubble nucleation is not only a function of the saturation level of the solution but also of the size of the brine channel. Thus, a minimum brine channel size may be required to form a stable bubble. Bubble nucleation should be successful for bubbles with radii sufficiently large so that the surface tension is smaller than the internal tension of the brine [*Light et al*., 2003]. On the other hand, the majority of bubbles observed by *Light et al*. [2003] were contained within brine inclusions, and none were observed in the ice itself. Although the gases we measured were primarily in the bubble phase, this does not exclude aqueous diffusion through the brine medium. If the bubbles are contained within the brine inclusions, the gas-filled inclusions are able to exchange gas with the brine and diffuse into the aqueous phase of the brine network. A possible connection, and exchange, between gas-filled and liquid-filled porosities has also been suggested by *Loose et al*. [2011].

The diffusivity of Ar and O_2 showed similar transport coefficients and the same trend over time. The values are also similar to those of *Wise and Houghton* [1966] in water at 10°C (salinity not specified), 1.7 $\times$ 10^{-5} cm^2 s^{-1}. However, the calculated D_{O_2} values are about 2 times lower than those reported (3.9 $\times$ 10^{-5} cm^2 s^{-1} ±41%) by *Loose et al*. [2011] for sea ice with similar porosities. Sea ice is a particularly heterogeneous environment, and the geometry and tortuosity of the channels would be expected to have a substantial influence on gas migration, especially in the form of bubble buoyancy. This is supported by the slight increase of *D* over time, which may be related to the increasing brine volume allowing easier diffusion and/or easier bubbles buoyancy. Therefore, it is not surprising that our values

differ from those of *Loose et al*. [2011]. It also suggests that it may be desirable to establish a relationship between porosity and molecular diffusion, but the available data do not cover a wide enough range of values to make this feasible.

As mentioned previously, the calculated value of D_{N_2} was higher than D_{O_2} and D_{Ar}. However, according to *Broecker and Peng* [1974] and *Stauffer et al*. [1985], D_{N_2} would be expected to be lower than D_{O_2}. Moreover, the peak decreased less symmetrically. *Loose et al*. [2011] suggest a multiphase diffusion where transport of a part of the gas occurs by liquid diffusion and another part by gas diffusion or by bubble buoyancy. This may accelerate the depletion of the gas fraction because the bubble buoyancy is much faster than aqueous diffusion. Based on the solubility coefficient (i.e., Bunsen, β), the gas species with the lowest solubility will be enriched in the gas phase; which is referred to as "solubility partitioning." O_2 is twice as soluble in water compared with N_2, and so the ability of N_2 to partition to the gas phase more readily would provide it with a more rapid transport pathway and hence higher "apparent" diffusivities with an assymetric evolution of the gas peak. Note that this solubility partitioning could also be involved in the chemical separation in the boundary layer during the ice growth. Thus, the supersaturation level to initiate the nucleation process would be reached earlier for N_2. The growing ice would be enriched in nitrogen bubbles that would otherwise have diffused as a solute toward the water reservoir. It is, however, not clear yet how such boundary layer processes are compatible with the mushy layer approach for sea ice growth.

6. Conclusion

Our study investigated the transport of gas in natural sea ice in the absence of brine convection. The low average bulk ice salinity (3.2) induced a stratified brine network, which prevented convective exchanges trough brines transport between the ice, water, and atmosphere. Hence, the transport of gas species was mainly diffusive or buoyant. We used the temporal evolution of gas distribution in sea ice to compute the bulk ice transport coefficients for Ar, N_2, and O_2 as conservative dissolved gas tracers of mass transport.

Based on the total gas content (i.e., included dissolved or gaseous gas species), the bulk ice concentration of O_2, N_2, and Ar, and the gas-filled porosity, we conclude that gas species are preferentially located in bubbles. The gas incorporation at the ice-water interface occurred close to the atmospheric solubility value, and the gas-filled porosity was close to zero in the bottom of the ice, hence, the nucleation process occurred mainly in the brines. Bubble nucleation requires supersaturation of dissolved gas in the brines, and in this study the nucleation process was observed once the concentration exceed 2.7 times the atmospheric saturation. This level of supersaturation is in agreement with previous work on bubble nucleation in sea ice [e.g., *Killawee et al*., 1998].

The effective gas diffusion rates through sea ice observed in this study ranged from 1.54 to 1.76 $\times 10^{-5}$ $cm^2\ s^{-1}$ ($\pm$17%) for Ar, from 1.54 to 1.77 $\times 10^{-5}$ $cm^2\ s^{-1}$ ($\pm$11%) for O_2, and was 2.49 $\times 10^{-5}$ $cm^2\ s^{-1}$ ($\pm$8%) for N_2. We computed this transport rate over a narrow range of total porosity, 4–8%. It was therefore not possible to ascertain a relationship between porosity and the diffusion coefficient; however, these experiments give some idea of the magnitude of D close the liquid permeability threshold of 5%.

Although most gases were located in bubbles, the effective diffusivities for O_2, Ar, and N_2 were close to the aqueous diffusion rate ($\approx 10^{-5}$ $cm^2\ s^{-1}$). The preference for gases to exist in bubbles does not exclude an aqueous diffusion through the brine medium. The majority of bubbles observed by *Light et al*. [2003] were contained within brine inclusions; none were observed in the ice itself. We hypothesize that the nucleation process occurs in the brine network and the gas-filled inclusions are able to exchange with the brine and diffuse into the aqueous phase. This work therefore extends to natural sea ice, the hypothesis that there is a connection and exchange between gas-filled porosity and liquid-filled porosity, previously suggested by *Loose et al*. [2011]. Finally, the preferential partitioning of N_2 into gas-filled pore spaces within the ice could produce a greater apparent diffusion rate in comparison to O_2 and Ar, as well as a larger rate of incorporation at the ice-water interface during the initial freezing process.

Acknowledgments
We gratefully acknowledge the contributions of the Canada Excellence Research Chair (CERC) and Canada Research Chair (CRC) programs. Support was also provided by the Natural Sciences and Engineering Research (NSERC) Council, the Canada Foundation for Innovation, and the University of Manitoba. This work is a contribution to the ArcticNet Networks of Centres of Excellence and the Arctic Science Partnership (ASP) *asp-net.org*. This work is also a contribution to the Belgian FNRS-FRFC 2.4584.09 research contract. B.D. is a research associate of F.R.S.-FNRS. Participation by D.N.T. was made possible by The Royal Society, U.K. The authors would like to thank Saïda El Amri for her efficient help in laboratory work.

References

Broecker, W. S., and T. H. Peng (1974), Gas-exchange rates between air and sea, *Tellus*, *26*(1-2), 21–35.
Carte, A. E. (1961), Air bubbles in ice, *Proc. Phys. Soc. London*, *77*(495), 757–768.
Cassar, N., B. A. Barnett, M. L. Bender, J. Kaiser, R. C. Hamme, and B. Tilbrook (2009), Continuous high-frequency dissolved O-2/Ar measurements by equilibrator inlet mass spectrometry, *Anal. Chem.*, *81*(5), 1855–1864.

Castro-Morales, K., N. Cassar, D. R. Shoosmith, and J. Kaiser (2013), Biological production in the Bellingshausen Sea from oxygen-to-argon ratios and oxygen triple isotopes, *Biogeosciences*, *10*(4), 2273–2291.

Cox, G. F. N., and W. F. Weeks (1983), Equations for determining the gas and brine volumes in sea-ice samples, *J. Glaciol.*, *29*(102), 306–316.

Crabeck, O., B. Delille, D. N. Thomas, N. X. Geilfus, S. Rysgaard, and J. L. Tison (2014), CO_2 and CH_4 in sea ice from a subarctic fjord, *Biogeosci. Discuss.*, *11*, 4047–4083, doi:10.5194/bgd-11-4047-2014.

Cussler, E. L. (2009), *Diffusion, Mass Transfert in Fluid System*, 3rd ed., Cambridge Univ. Press, N.Y.

Eicken, H., M. A. Lange, and G. S. Dieckmann (1991), Spatial variability of sea ice properties in the Northwestern Weddell Sea, *J. Geophys. Res.*, *96*(C6), 10,603–10,615.

Else, B. G. T., T. N. Papakyriakou, R. J. Galley, W. M. Drennan, L. A. Miller, and H. Thomas (2011), Wintertime CO_2 fluxes in an Arctic polynya using eddy covariance: Evidence for enhanced air-sea gas transfer during ice formation, *J. Geophys. Res.*, *116*, C00G03, doi:10.1029/2010JC006760.

Garcia, H. E., and L. I. Gordon (1992), Oxygen solubility in seawater—Better fitting equations, *Limnol. Oceanogr.*, *37*(6), 1307–1312.

Geilfus, N.-X., G. Carnat, T. Papakyriakou, J.-L. Tison, B. Else, H. Thomas, E. Shadwick, and B. Delille (2012), Dynamics of pCO_2 and related air-ice CO_2 fluxes in the Arctic coastal zone (Amundsen Gulf, Beaufort Sea), *J. Geophys. Res.*,*117*, C00G10, doi:10.1029/2011JC007118.

Geilfus, N.-X., G. Carnat, G. S. Dieckmann, N. Halden, G. Nehrke, T. Papakyriakou, J.-L. Tison, and B. Delille (2013), First estimates of the contribution of $CaCO_3$ precipitation to the release of CO_2 to the atmosphere during young sea ice growth, *J. Geophys. Res. Oceans*, *118*, 244–255, doi:10.1029/2012JC007980.

Golden, K. M., S. F. Ackley, and V. I. Lytle (1998), The percolation phase transition in sea ice, *Science*, *282*(5397), 2238–2241.

Golden, K. M., H. Eicken, A. L. Heaton, J. Miner, D. J. Pringle, and J. Zhu (2007), Thermal evolution of permeability and microstructure in sea ice, *Geophys. Res. Lett.*, *34*, L16501, doi:10.1029/2007GL030447.

Gosink, T. A., J. G. Pearson, and J. J. Kelly (1976), Gas movement through sea ice, *Nature*, *263*, 41–42.

Hamme, R. C., and S. R. Emerson (2004), The solubility of neon, nitrogen and argon in distilled water and seawater, *Deep Sea Res., Part I*, *51*(11), 1517–1528.

Heinesch, B., M. Yernaux, M. Aubinet, N. X. Geilfus, T. Papakyriakou, G. Carnat, H. Eicken, J. L. Tison, and B. Delille (2009), Measuring air-ice CO_2 fluxes in the Arctic, *FluxLetter*, *2*(2), 9–10.

Kaartokallio, H., D. H. Sogaard, L. Norman, S. Rysgaard, J. L. Tison, B. Delille, and D. N. Thomas (2013), Short-term variability in bacterial abundance, cell properties, and incorporation of leucine and thymidine in subarctic sea ice, *Aquat. Microbial Ecol.*, *71*(1), 57–73.

Killawee, J. A., I. J. Fairchild, J. L. Tison, L. Janssens, and R. Lorrain (1998), Segregation of solutes and gases in experimental freezing of dilute solutions: Implications for natural glacial systems, *Geochim. Cosmochim. Acta*, *62*(23-24), 3637–3655.

Langway, C. C. (1958), Ice fabrics and the universal stage, *Rep. 62*, U.S. Snow, Ice and Permafrost Res. Estab., Wilmette, Ill.

Leppäranta, M., and T. Manninen (1988), The brine and gas content of sea ice with attention to low salinities and high temperatures, Finnish Institute of Marine Research, 15 pp, report 2, Helsinki, Finland.

Light, B., G. A. Maykut, and T. C. Grenfell (2003), Effects of temperature on the microstructure of first-year Arctic sea ice, *J. Geophys. Res.*, *108*(C2), 3051, doi:10.1029/2001JC000887.

Long, M. H., D. Koopmans, P. Berg, S. Rysgaard, R. N. Glud, and D. H. Sogaard (2012), Oxygen exchange and ice melt measured at the ice-water interface by eddy correlation, *Biogeosciences*, *9*, 1–11.

Loose, B., W. R. McGillis, P. Schlosser, D. Perovich, and T. Takahashi (2009), Effects of freezing, growth, and ice cover on gas transport processes in laboratory seawater experiments, *Geophys. Res. Lett.*, *36*, L05603, doi:10.1029/2008GL036318.

Loose, B., P. Schlosser, D. Perovich, D. Ringelberg, D. T. Ho, T. Takahashi, J. Richter-Menge, C. M. Reynolds, W. R. McGillis, and J. L. Tison (2011), Gas diffusion through columnar laboratory sea ice: Implications for mixed-layer ventilation of CO2 in the seasonal ice zone, *Tellus, Ser. B*, *63*(1), 23–39.

Lubetkin, S. D. (2003), Why is it much easier to nucleate gas bubbles than theory predicts?, *Langmuir*, *19*, 2575–2587.

Matsuo, S., and Y. Miyake (1966), Gas composition in ice samples from Antarctica, *J. Geophys. Res.*, *71*(22), 5235–5241.

Miller, L. A., T. N. Papakyriakou, R. E. Collins, J. W. Deming, J. K. Ehn, R. W. Macdonald, A. Mucci, O. Owens, M. Raudsepp, and N. Sutherland (2011), Carbon dynamics in sea ice: A winter flux time series, *J. Geophys. Res.*, *116*, C02028, doi:10.1029/2009JC006058.

Mortensen, J., K. Lennert, J. Bendtsen, and S. Rysgaard (2011), Heat sources for glacial melt in a sub-Arctic fjord (Godthåbsfjord) in contact with the Greenland Ice Sheet, *J. Geophys. Res.*, *116*, C01013, doi:10.1029/2010JC006528.

Nomura, D., H. Yoshikawa-Inoue, and T. Toyota (2006), The effect of sea-ice growth on air-sea CO_2 flux in a tank experiment, *Tellus, Ser. B*, *58*(5), 418–426.

Nomura, D., H. Yoshikawa-Inoue, T. Toyota, and K. Shirasawa (2010), Effects of snow, snow-melting and re-freezing processes on air-sea ice CO_2 flux, *J. Glaciol.*, *56*(196), 262–270.

Notz, D., and M. G. Worster (2008), In situ measurements of the evolution of young sea ice, *J. Geophys. Res.*, *113*, C03001, doi:10.1029/2007JC004333.

Papadimitriou, S., H. Kennedy, L. Norman, D. P. Kennedy, G. S. Dieckmann, and D. N. Thomas (2012), The effect of biological activity, $CaCO_3$ mineral dynamics, and CO_2 degassing in the inorganic carbon cycle in sea ice in late winter-early spring in the Weddell Sea, Antarctica, *J. Geophys. Res.*, *117*, C08011, doi:10.1029/2012JC008058.

Papakyriakou, T., and L. Miller (2011), Springtime CO_2 exchange over seasonal sea ice in the Canadian Arctic Archipelago, *Ann. Glaciol.*, *52*(57), 215–224.

Raynaud, D., R. Delmas, M. Ascencio, and M. Legrand (1982), Gas extraction from polar ice cores: A critical issue for studying the evolution of atmospheric CO_2 and ice-sheet surface elevation, *Ann. Glaciol.*, *3*, 265–268.

Rysgaard, S., and R. N. Glud (2004), Anaerobic N-2 production in Arctic sea ice, *Limnol. Oceanogr. Methods*, *49*(1), 86–94.

Rysgaard, S., R. N. Glud, M. K. Sejr, J. Bendtsen, and P. B. Christensen (2007), Inorganic carbon transport during sea ice growth and decay: A carbon pump in polar seas, *J. Geophys. Res.*, *112*, C03016, doi:10.1029/2006JC003572.

Shaw, M. D., L. J. Carpenter, M. T. Baeza-Romero, and A. V. Jackson (2011), Thermal evolution of diffusive transport of atmospheric halocarbons through artificial sea-ice, *Atmos. Environ.*, *45*(35), 6393–6402.

Skoog, D. A., D. M. West, and F. J. Holler (1997), *Chimie Analytique*, De Boeck Univ., Paris.

Sogaard, D. H., D. N. Thomas, S. Rysgaard, R. N. Glud, L. Norman, H. Kaartokallio, T. Juul-Pedersen, and N. X. Geilfus (2013), The relative contributions of biological and abiotic processes to carbon dynamics in subarctic sea ice, *Polar Biol.*, *36*(12), 1761–1777.

Sørensen, L. L., B. Jensen, R. N. Glud, D. F. McGinnis, M. K. Sejr, J. Sievers, D. H. Søgaard, J.-L. Tison, and S. Rysgaard, (2013), Parameterization of atmosphere–surface exchange of CO_2 over sea ice, *Cryosphere Discuss.*, *7*, 3899–3929, doi:10.5194/tcd-7-3899-2013.

Stauffer, B., A. Neftel, H. Oeschger, and J. Schwander (Eds.) (1985), *CO_2 Concentration in Air Extracted From Greenland Ice Samples, Geophys. Monogr. Ser.*, 85–89 pp., AGU, Washington, D. C.

Stefels, J., G. Carnat, J. W. H. Dacey, T. Goossens, J. T. M. Elzenga, and J. L. Tison (2012), The analysis of dimethylsulfide and dimethylsulfoniopropionate in sea ice: Dry-crushing and melting using stable isotope additions, *Mar. Chem.*, *128–129*, 34–43.

Tison, J. L., C. Haas, M. M. Gowing, S. Sleewaegen, and A. Bernard (2002), Tank study of physico-chemical controls on gas content and composition during growth of young sea ice, *J. Glaciol.*, *48*(161), 177–191.

Tison, J. L., A. Worby, B. Delille, F. Brabant, S. Papadimitriou, D. Thomas, J. de Jong, D. Lannuzel, and C. Haas (2008), Temporal evolution of decaying summer first-year sea ice in the Western Weddell Sea, Antarctica, *Deep Sea Res., Part I*, *55*(8-9), 975–987.

Tsurikov, V. L. (1979), The formation and composition of the gas content of sea ice, *J. Glaciol.*, *22*(86), 67–81.

UNESCO (1978), Eight report of the joint panel on oceanographic tables and standards, *UNESCO Tech. Pap. Mar. Sci., 28*.

Vancoppenolle, M., H. Goosse, A. de Montety, T. Fichefet, B. Tremblay, and J. L. Tison (2010), Modeling brine and nutrient dynamics in Antarctic sea ice: The case of dissolved silica, *J. Geophys. Res.*, *115*, C02005, doi:10.1029/2009JC005369.

Wise, D. L., and G. Houghton (1966), Diffusion coefficients of 10 slightly soluble gases in water at 10–60 degrees c, *Chem. Eng. Sci.*, *21*(11), 999–1010.

Zemmelink, H. J., B. Delille, J. L. Tison, E. J. Hintsa, L. Houghton, and J. W. H. Dacey (2006), CO_2 deposition over the multi-year ice of the western Weddell Sea, *Geophys. Res. Lett.*, *33*, L13606, doi:10.1029/2006GL026320.

Zhou, J. Y., B. Delille, H. Eicken, M. Vancoppenolle, F. Brabant, G. Carnat, N. X. Geilfus, T. Papakyriakou, B. Heinesch, and J. L. Tison (2013), Physical and biogeochemical properties in landfast sea ice (Barrow, Alaska): Insights on brine and gas dynamics across seasons, *J. Geophys. Res. Oceans*, *118*, 3172–3189, doi:10.1002/jgrc.20232.